Electron Beam Induced Modification of N-Heterocyclic Carbenes – Carbon Nanomembrane Formation

Daria M. Cegiełka,[1,2] Martha Frey,[3] Krzysztof Kozieł,[4] Christof Neumann,[3] Andrey Turchanin[3,5] and Piotr Cyganik[1]**

[1]Jagiellonian University, Faculty of Physics, Astronomy and Applied Computer Science, Smoluchowski Institute of Physics, Łojasiewicza 11, 30-348 Krakow, Poland.

[2]Jagiellonian University, Doctoral School of Exact and Natural Sciences, Łojasiewicza 11, 30-348 Krakow, Poland

[3]Institute of Physical Chemistry, Friedrich Schiller University Jena, Lessingstraße 10, 07743 Jena, Germany

[4]Faculty of Chemistry, Jagiellonian University, 30-387 Krakow, Poland

[5]Jena Center for Soft Matter, 07743 Jena, Germany

*corresponding authors: piotr.cyganik@uj.edu.pl, andrey.turchanin@uni-jena.de

KEYWORDS: N-heterocyclic carbenes, self-assembled monolayers, electron irradiation, carbon nanomembrane.

Abstract

Electron irradiation of self-assembled monolayers (SAMs) is a versatile tool for a variety of lithographic methods and formation of new 2D materials such as carbon nanomembranes (CNMs) with potential application in ultrafiltration. While the interaction between the electron beam and standard aromatic or aliphatic thiolate SAMs on gold has been well studied, the behavior of more complex systems such as N-heterocyclic carbenes (NHCs), which are recently attracting growing attention due to their ultra-high chemical and thermal stability, remains completely unknown. In the current work, we analyze the low-energy electron irradiation of SAMs on gold based on the series of NHC molecules featuring different number of benzene moieties (0, 1 and 2), and different size of the nitrogen side groups (methyl, isopropyl) to modify their packing density. The changes in monolayer thickness and composition are carefully analyzed by the X-ray photoelectron spectroscopy (XPS) as a function of electron dose. Our results provide design rules to optimize NHC SAMs structure for their effective modification by the electron irradiation. Such optimization becomes particularly interesting considering that the analyzed NHC monolayers exhibit a much higher stability of their bonding with the metal substrate towards electron irradiation compared to standard thiols or recently applied carboxylic acids. Thus, the NHC SAMs offer an interesting alternative for chemical lithography where structural modification of SAMs by electron or photon beams should be limited mainly to the functional group. Moreover, delamination and transferring of electron irradiated NHC monolayers on holey TEM grid reveals formation of carbon nanomembranes (CNMs). As we show this process is also very sensitive to the structure of NHC SAMs and for properly designed system enables formation of continuous, freestanding CNMs, which are sulfur free and thus much more suitable for some ultrafiltration applications compared to standard CNMs fabricated from thiols and therefore contaminated with reactive sulfur.

1. Introduction

Self-assembled monolayers (SAMs) form well-defined organic nanostructures on inorganic substrates by spontaneous chemisorption.[1–3] The ease of SAM formation provides a simple and extremely effective method for surface/interface functionalization which was recently recognized by awarding SAMs discoverers by Kavli Award in Nanoscience.[4] This functionalization process becomes particularly robust in combination with several pattering methods of SAMs[5] which were applied mainly for building organic electronic devices[6–12] and controlling biocompatible interfaces towards the design of new sensors and tissue engineering.[13–16] In particular, electron-beam irradiation allows for well-defined modification of SAM structure, and thus related surface/interface functionalization *via* several different processes that include partial desorption of monolayer,[17–19] cross-linking of molecules within the monolayer,[20–24] and [24]modification of their chemical functionality.[25–29] These electron-beam stimulated processes can be operated from micrometer down to nanometer scale, and were already applied for a few different types of lithography,[25,28,30–35] work function adjustment,[36] and formation of carbon-based materials such as graphene[37,38] or carbon nanomembranes (CNMs).[39–43] Generally, over the last 25 years most applications related to electron irradiation of SAMs were based on using mainly aromatic or aliphatic thiols on gold substrate. Only recently, another approach was taken by us[44,45] and others[46,47] using SAMs with carboxylic anchoring group formed on silver substrate. It was demonstrated that this type of SAMs can be applied for the formation of sulfur-free CNMs[44] which can be favorable for some ultrafiltration process.[48,49] A disadvantage of this system is however a much lower stability of carboxylic bonding group towards electron irradiation compared to standard thiols,[45] which may impair certain applications, especially those where irradiation should lead only to chemical modification of SAMs functionality and/or structure without pronounced film desorption.[27,34,36,50,51]

Searching for monolayers, which are sulfur-free but at the same time exhibit high stability of their bonding group towards electron irradiation one could consider N-heterocyclic carbenes (NHC) as a potential candidate. The NHC-based SAMs on gold, with the carbene carbon atom as a bonding group, were widely explored in recent years revealing extremely high chemical,[52] electrochemical[52–54] and thermal[53,55–57] stability compared to standard thiols on the same substrate. All these stability-related parameters are obviously crucial for most of possible applications, and therefore, intensive research of NHC SAMs structure, properties, and possible applications was undertaken as documented in literature.[58–61] To the best of our knowledge, up to now, however, the interaction of NHC SAMs with electron irradiation has not been analyzed. As argued above, optimization of electron-induced modification of a given type of SAMs opens a wide range of their possible applications. Considering structural modifications introduced by the NHC SAMs compared to standard monolayers based on thiols or carboxylic acids *i.e.* the new type of surface anchoring group in combination with N-heterocyclic structure of the molecular backbone, such analysis for NHC SAMs seems also crucial from the viewpoint of fundamental mechanisms of electron interaction with organic films.

To this end in the current study, we analyze low-energy (50 eV) electron irradiation for a series of well-ordered, densely packed, model NHC SAMs on gold with systematically modified molecular structure (**Figure 1**). Our experiments indicate not only much higher stability of the carbene bonding group towards electron irradiation as compared to thiols but also electron-beam stimulated formation of new chemical bonds with the substrate. Moreover, we also demonstrate that for properly designed NHC SAMs, successful sulfur-free CNM formation can be achieved.

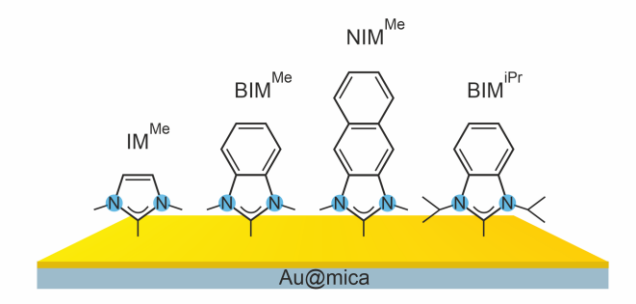

Figure 1. Schematic presentation of NHC molecules used for this study together with respective acronyms.

2. Experimental Methods

2.1 SAM Preparation. The synthetic protocols for all NHC compounds (*i.e.* IM, BIM^{Me}, BIM^{iPr} and NIM) used in this study (schematically presented in **Figure 1)** can be found elsewhere.[57] All NHC SAMs on Au(111) have been prepared strictly following former spectroscopic characterization of these systems.[57] In short, the Au(111) substates were prepared at 300 ^{o}C by evaporation of ~100 nm (rate ~0.15 nm/s) of gold on freshly cleaved mica (grade V1, Ted Pella USA). Prior to the evaporation, the mica substrate was annealed at evaporation temperature for ~15 h to remove contaminations. Respective SAMs were prepared by immersion (~20 h) of Au(111) substrates in the solution (1 mM) of the respective compound in THF (anhydrous, Sigma-Aldrich) which was degassed prior to the incubation (5-6 cycles of freeze-pump-thaw procedure in the Schlenk apparatus). The incubation of samples was conducted at RT under controlled argon atmosphere in the glovebox (MBraun). Directly before analysis samples were taken out from solution, rinsed (pure THF) and dried under nitrogen stream.

2.2 Electron Irradiation. The irradiation experiments were performed using 50 eV electron beam generated by the NEK-SC 150 (Staib) electron gun in the same ultra-high vacuum system as used for the XPS analysis.

2.3 X-ray Photoelectron Spectroscopy (XPS). The analysis was conducted *in situ* using ultra-high vacuum (UHV, base pressure 2 x 10^{-10} mbar) system (Scienta Omicron) equipped with monochromatic X-ray source (Al K_α) and electron energy analyzer (Argus CU) working at 0.6 eV spectral energy resolution. For the calibration of binding energy (BE) scale, the Au $4f_{7/2}$ peak (BE = 84.0 eV) was used. For fitting obtained XP spectra Voigt functions were used after background subtraction using linear (N 1s) or Shirley (C 1s, Au 4f) function.

2.4 The CNM formation. The transfer of CNMs on TEM grids (Quantifoil R 2/2 on Cu, 400 mesh) was performed following protocol described previously.[44] In short the process consist of several consecutive steps that include: (1) spin-casting of poly(methyl methacrylate) (PMMA) on CNM/Au sample and baking on a hotplate at 90 °C for 5 min, (2) spin-casting second PMMA layer followed by baking with the same parameters, (3) electrochemical delamination (in NaOH, voltage of 2−3 V) of CNM from the Au substrate, (4) transferring the CNM/PMMA sandwich on TEM grid after cleaning the sample in ultrapure water, (5) drying at 50 °C for 1 h on a hotplate, (6) immersion in acetone followed by rinsing with isopropanol to remove the PMMA layer and (7) critical point drying (Autosamdri-815, Tousimis).

2.3. Scanning Electron Microscopy (SEM). The Zeiss Sigma VP field emission scanning electron microscope was used for collecting SEM images using the in-lens detector and an electron beam energy of 15 kV.

3. Results and Discussion

The electron irradiation experiments were performed for series of NHC monolayers containing imidazolium (IM) moiety to link molecules with the gold substrate, which, with only few exceptions,[62–64] is currently the most common strategy for NHC SAM formation.[54,58–61,65–67] In analyzed series of molecules the IM moiety was linked with different number (*n*) of benzene rings: IM^{Me} (*n* = 0), BIM^{Me}/BIM^{iPr} (*n* = 1) and NIM^{Me} (*n* = 2). Importantly, in most of the here analyzed systems (IM^{Me}, BIM^{Me} and NIM^{Me}) short methyl (Me) side groups of nitrogen hereto atoms were used. Recent structural analysis of these monolayers[57] demonstrated that, in contrast to conclusions reached by former studies,[55,68–73] NHC molecules with short Me side groups can form densely packed, upright oriented, monolayers on Au(111) substrate. To determine possible impact of NHC with more bulky side groups, we also analyzed BIM^{iPr} which is the analogue of BIM^{Me} with isopropanol (iPr) side groups forming monolayers with roughly twice lower packing density.[57,69]

The electron irradiation of NHC SAMs formed by molecules presented in **Figure 1** was monitored *in situ* using XPS analysis conducted for progressively increased irradiation dose. The series of C 1s spectra obtained for BIM^{Me}/Au monolayer are presented in **Figure 2** as a representative example for all here analyzed NHC SAMs. The non-irradiated BIM^{Me}/Au SAM is characterized by an asymmetric C 1s peak with the maximum of the envelope located at the binding energy (BE) of ~285.2 eV. As discussed in our previous study[56,57] this asymmetry is related to the presence of two main components related to the imidazolium moiety (~286 eV) and the phenyl ring (~285 eV). We note that BE associated with the phenyl component is shifted by ~0.9 eV towards higher energy, compared to data known for aromatic thiol or selenol-based SAMs (~284.1 eV).[74–77] Following former analysis[56,57] we attribute the shift of this component to an electrostatic effect[78] caused by formation of the dipole layer at the molecule-metal interface upon modification of the bonding group from thiols to carbene. The

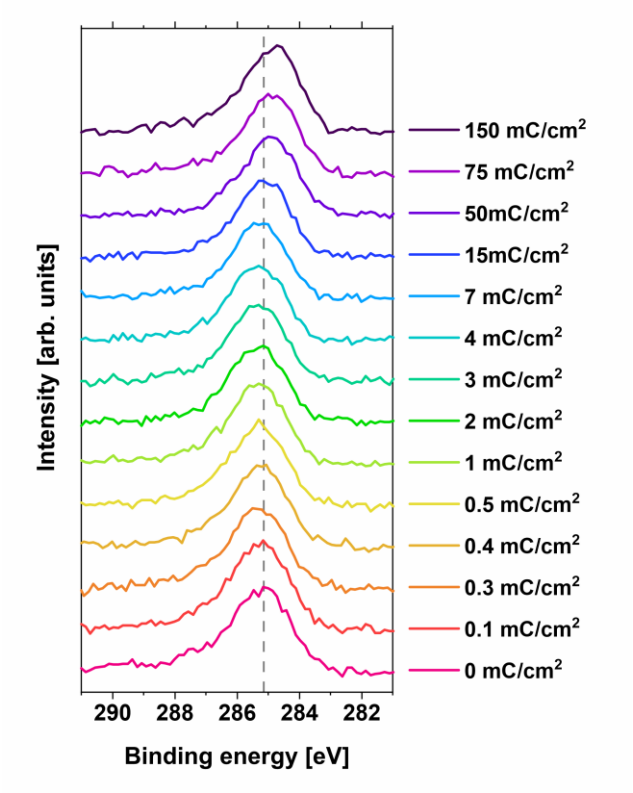

Figure 2. C 1s XPS data for electron-beam (50 eV) irradiated BIM^{Me}/Au monolayers using different total electron doses in the range 0-150 mC/cm^2. The grey dashed line indicates peak position for non-irradiated (native) sample.

observed shift towards higher BE values would then require an upward orientation of such dipole layer (with the respect of the Au substrate) which is consistent with the theoretically expected charge rearrangement upon C–Au bond formation (positive charge located at the carbene carbon atom)[79,80] and former secondary ion mass spectrometry (SIMS) analysis.[56,57]

As shown in **Figure 2**, the progressive irradiation of NHC SAMs, up to the dose of 150 mC/cm^2, leads to modification of both intensity and position of the C 1s peak. The systematic analysis of the film thickness (calculated by standard approach based on C 1s/Au 4f intensity ratio)[19,45,57] as a function of the irradiation dose Q/S [C/m^2] is presented in **Figure 3a** (see **Figure S1** for all

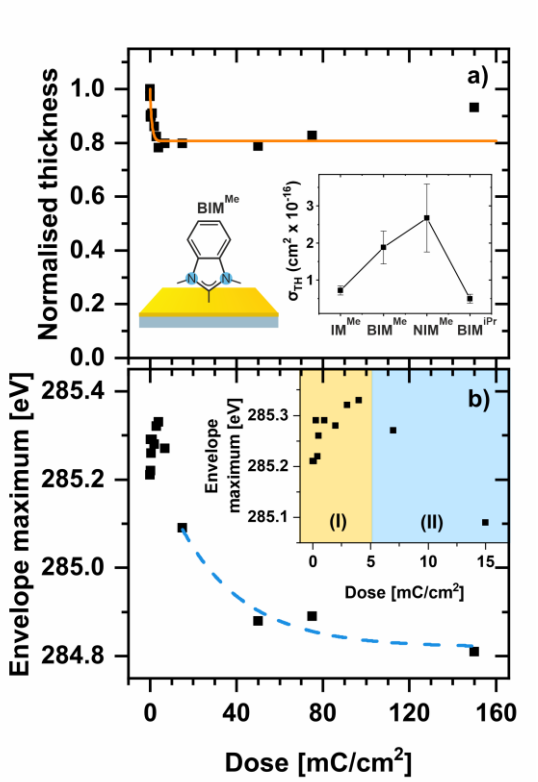

Figure 3. C 1s XPS data analysis for electron beam (50 eV) irradiated NHC SAMs. In (a) normalized film thickness of BIM^{Me}/Au monlayer as a function of the total electron dose with indicated (orange line) fitting of the saturation function (Eq. 1) - the inset shows calculated cross-sections for thickness modification (σ_{TH}) obtained for all analyzed NHC SAMs. In (b) BE of C 1s peak (envelope) maximum as a function of the total electron dose for BIM^{Me}/Au - the inset shows close-up for low doses indicating increase (by the cross-linking process – yellow range) and decrease (by the Au–C bond termination – blue range) of the BE value. The blue dashed line in (b) shows fitting of the saturation function (an analogue of Eq. 1) to the data in the range 15-150 mC/cm^2 where the Au–C bond termination process takes place (see text for details).

NHC SAMs) and reveals reduction of this parameter which, when normalized to the native film thickness d_0, can be described by the following saturation function:[18,19,22,45,81]

$$\frac{d(Q/S)}{d_0} = \frac{d_{SAT}}{d_0} + \frac{(d_0 - d_{SAT})}{d_0} \cdot exp\left(\frac{-\sigma_{TH} \cdot Q}{e \cdot S}\right), \quad (1)$$

where d_{SAT} and σ_{TH} are the thicknesses for the extensively irradiated monolayer (saturation value) and the cross-section for this process, respectively. The fraction of thickness reduction $(d_0 - d_{SAT})/d_0$ and σ_{TH} parameters obtained for analyzed here series of NHC SAMs are summarized in **Table 1**. We observe ~20% thickness reduction for all NHC SAMs except NIM^{Me}/Au for which the value of ~10% was estimated. Generally, the process of electron irradiation induced thickness reduction of SAMs is a consequence of competition of two main processes *i.e.* (i) scission of existing chemical bonds within molecules (*e.g.* C–H and C–C), followed by the desorption of respective fragments, and (ii) formation of new C–C/C=C bonds between neighboring molecules and thus cross-linking monolayer structure which is stabilizing it towards further desorption. For electron irradiation (50 eV) of aliphatic thiols on gold substantial reduction of SAMs thickness by ~40% was reported,[18,19] indicating dominant role of the desorption process. In contrast, for purely aromatic thiols on gold, the reported reduction of film thickness (under the same electron irradiation conditions) is much lower and, depending on the specific system, thickness reductions between nearly zero level (within the precision of such measurements ~5 %) and ~25% were reported,[81,82] confirming the dominant role of the cross-linking process in this case. Therefore, concerning ~10-20% thickness reduction for analyzed here NHC monolayers, we conclude dominant contribution of the cross-linking process for this type of SAMs as well. Importantly, we note that even for the IM^{Me}/Au monolayer, which does not contain a phenyl ring, the N-heterocyclic moiety alone provides efficient cross-linking of this monolayer with the reduction of film thickness (~20%). This value is even lower compared to the value (~25%) reported[82] under the same irradiation conditions for biphenyl thiols on gold - the archetypical SAMs for electron-based lithography[25,30,32] and carbon based materials formation.[37,39–43]

Table 1. Overview of the parameters for the analyzed NHC SAMs.

Parameter		IM^{Me}	BIM^{Me}	NIM^{Me}	BIM^{iPr}
σ_{TH} (cm^2 x 10^{-16})		0.7(0.1)	1.9(0.4)	2.7(0.9)	0.5(0.1)
σ_{C-Au} (cm^2 x 10^{-18})	from C 1s	2.9(0.6)	5.4(3.2)	1.6(0.2)	4.0(1.4)
	from N 1s	5.0(0.8)	6.2(1.2)	1.4(0.2)	2.5(1.6)
Thickness reduction (%)		20(7)	19(8)	10(7)	24(7)
ΔBE		0.70(0.1)	0.52(0.1)	0.54(0.1)	0.77(0.1)

The lowest reduction of the film thickness (~10%) was observed for NIM^{Me}/Au which is most probably related to the longest structure, and thus, the highest probability for the cross-linking during the transition of electrons (primary and secondary) through the thickest monolayer. This assumption is also fully consistent with the highest value of the cross-section for the thickness modification for NIM^{Me}/Au among all here analyzed NHC monolayers (see the inset in **Figure 2a** and the data in **Table 1**). The higher the value of σ_{TH}, the lower is the dose of electron irradiation needed to reach the saturation range of film thickness reduction associated with the completeness of the monolayer cross-linking process. The systematic increase in the value of σ_{TH} with elongations of the NHC molecules skeleton going from IM^{Me}/Au (~0.7 10^{-16} [cm^2]) to BIM^{Me}/Au (~1.9 10^{-16} [cm^2]) and NIM^{Me}/Au (σ_{TH} ~2.7 10^{-16} [cm^2]) confirms above argumentation (see inset in **Figure 3a**). This trend does not hold for BIM^{iPr}/Au monolayer showing a value of σ_{TH} (~0.5 10^{-16} [cm^2]) which is not only much lower compared to equally long analogues BIM^{Me}/Au but also lower than the value obtained for the shortest monolayer *i.e.* IM^{Me}/Au. However, this is only an apparent inconsistency; in fact, this result confirms the above model considering the much more bulky nitrogen side group of the molecules forming BIM^{iPr}/Au compared to all other analyzed here NHC SAMs. As pointed out earlier, the modification of this side group from Me to iPr leads to almost twice lower packing density,[57,69] thus hindering the cross-linking process taking place between neighboring molecules in the monolayer.

Another important parameter which traces the C 1s signal modification, and thus the electron-beam induced processes in NHC films, is the respective BE, which as a function of the irradiation dose is presented in **Figure 3b** and **Figure S2**. As exemplified by the data obtained for BIM^{Me}/Au, the modification of the BE for C 1s signal does not show monotonic behavior reported earlier for SAM with thiol[18,81] or carboxylic[45] bonding groups. The initial irradiation up to the dose of ~2-4 mC/cm^2 leads to an increase in the BE in the range of ~0.1-0.2 eV (see inset in **Figure 3b** and data shown in **Figure S2**). A similar increase of the C 1s BE induced by electron irradiation (50 eV) was reported in previous experiments for purely aromatic thiols on gold with a saturation point at ~10 mC/cm^2.[81] Following these former studies, we attribute the observed increase in the C 1s BE, which is not observed for purely aliphatic SAMs,[18] to the cross-linking process taking place in the NHC SAMs. We also note that in **Figure 3** the range of total electron dose where an increase in the C 1s BE was observed is the same as the range where the drop of the film thickness is taking place, which additionally supports above hypothesis considering that thickness modification is limited by the cross-linking process. However, in contrast to electron irradiation of all other SAMs, for NHC monolayers this initial, and relatively small, increase of C 1s BE for doses up to 3-4 mC/cm^2 is followed by a few times larger decrease of BE which saturates at the doses which exceed ~100 mC/cm^2. This observation indicates yet another process of NHC SAM modification which plays a dominant role for larger irradiation doses. Considering the direction of the BE shift towards lower values, such modification is most probably related to the elimination of the original C–Au bonds in the monolayer, which leads to destruction of the dipole layer formed upon chemisorption, and as a result, progressive shifting down the C 1s BE towards value which is typical for cross-linked aromatic thiol systems *i.e.* ~284.2 eV.[81] The C–Au bond termination as a function of electron dose can be described by the respective saturation function, similar as to thickness modification discussed above. To extract the corresponding cross-section for this process (σ_{C-Au}) we have

fitted respective data in the range from 15 to 150 mC/cm^2 *i.e.* in the region of electron dose where the cross-linking process is at the saturation stage, and further modification of the BE value is due to the Au–C bond termination process only (see blue dashed line in **Figure 3b and Figure S2**). The estimated values of σ_{C-Au} obtained for all NHC SAMs analyzed here are in the range of 10^{-18} cm^2 which is proximately one or two orders of magnitude lower than the corresponding cross-section values for the bonding group termination reported previously for thiols on gold substrate[19,81] and carboxylic acids on silver,[45] indicating thus significantly higher stability of the C–Au bond towards electron irradiation compared to S–Au or O–Ag.

The shifting of C 1s BE value towards lower values is directly related to the change in the potential energy step ΔV associated with the dipole layer formation, which from simple electrostatic considerations (omitting depolarization effects) is proportional to the surface density ρ of the dipole moments μ_{CAu} associated with the C–Au bond formation according to the following equation:[83–85]

$$\Delta V \approx -\rho \frac{\mu_{\perp CAu}}{\varepsilon_0 \varepsilon_{CAu}}, \quad (2)$$

where $\mu_{\perp CAu}$ is the normal component (to the metal substrate) of the μ_{CAu}, ε_0 is the vacuum permittivity, and ε_{CAu} is the dielectric constant at the C/Au interface. Therefore, the observed reduction in the BE (*ΔBE*) from maximal value of the BE (BE_{MAX}) down to minimal value (BE_{MIN}), both measured in **Figure 3b,** is proportional to the fraction of the C–Au bond eliminated during irradiation. The respective data summarized in **Table 1** show lower values of *ΔBE* parameter for BIM^{Me}/Au and NIM^{Me}/Au compared to IM^{Me}/Au and BIM^{iPr}/Au monolayers *i.e.* lower fraction of C–Au bonds terminated for the former monolayers. Concluded here higher stability of C–Au bond towards electron irradiation for BIM^{Me}/Au and NIM^{Me}/Au compared to IM^{Me}/Au and BIM^{iPr}/Au could be correlated with previous analysis[57] of these NHC SAMs showing much higher thermal stability for the former group of monolayers. Pronounced

difference in thermal stability originates most likely from the changes in the conformation of chemical bonds at the molecule–metal interface including the C–Au bond *e.g.* different orientation of this bond relative to the metal substrate and/or different configuration of the bonding to Au atom/adatom. The ionization and excitation processes induced by electron irradiation may lead to the formation of the repulsive state, and subsequently, to dissociation of the given chemical bond.[86,87] For chemical bonds located at the molecule–metal interface the probability of this dissociation process can be radically reduced by non-radiative relaxation of the respective repulsive state *via* two processes: (i) interaction of the oscillating dipole (representing excited repulsive state) and its image which leads to creation of phonon or electron-hole pair in the metal substrate and (ii) electron tunneling from this excited state to the metal substrate.[87] Since efficiency of both processes strongly depends on the distance between the excited bond and the metal surface as well as on the details of their electronic structure,[87] the modification of the bonding geometry of the NHC molecules will have pronounced impact on the stability of their C–Au bond towards electron irradiation as it was observed also for other types of SAMs)[22,45,86]

Electron induced modification of the NHC SAMs is also visible in the N 1s signal. In **Figure 4** representative example of such data for BIM^{Me}/Au is presented. For non-irradiated (native) NHC SAMs a single N 1s component was observed at ~400.4 eV except for IM^{Me}/Au where a slightly higher BE (~400.7 eV) value was measured in accordance with former analysis of these monolayers.[57] We note at this point that due to much lower abundance of nitrogen in NHC SAMs compared to carbon and higher attenuation of the emission for respective photo electrons, the signal to noise ratio for N 1s is significantly lower compared to C 1s, so the respective analysis is much less precise. However, the key aspects of

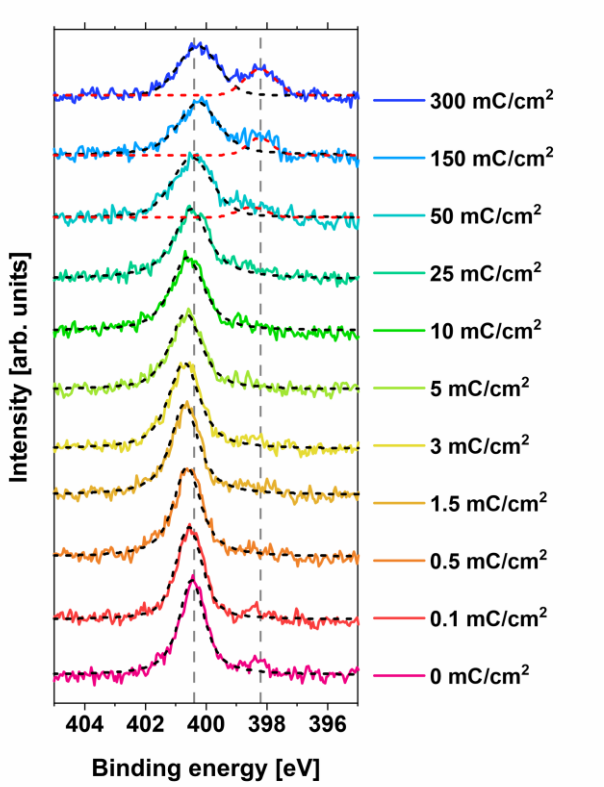

Figure 4. N 1s XPS data for electron-beam (50 eV) irradiated BIM^{Me}/Au monolayers using different total electron doses in the range 0-150 mC/cm^2. Grey dashed lines indicate: peak position (~400.4 eV) for non-irradiated (native) sample and position of the new peak (~398.3 eV) visible only at higher irradiation doses.

electron beam induced modification of NHC SAMs can be observed in the N 1s signal. As presented in **Figure 5a** and **Figure S3** whereas the total N 1s intensity remains essentially unchanged during the irradiation process (within the ~10% precision of our analysis), the intensity of the main component is reduced by ~20-25% upon reaching high electron doses (50-300 mC/cm^2) with, however, simultaneous appearance of a new component (red dashed line in **Figure 4a)**. This new component is located at ~398-399 eV and, considering former XPS data for SAMs on Au(111) with amine[88,89] or pyridine[90] anchoring group, can be associated with the N–Au bond formation. Although we cannot exclude that complete detachment of nitrogen from

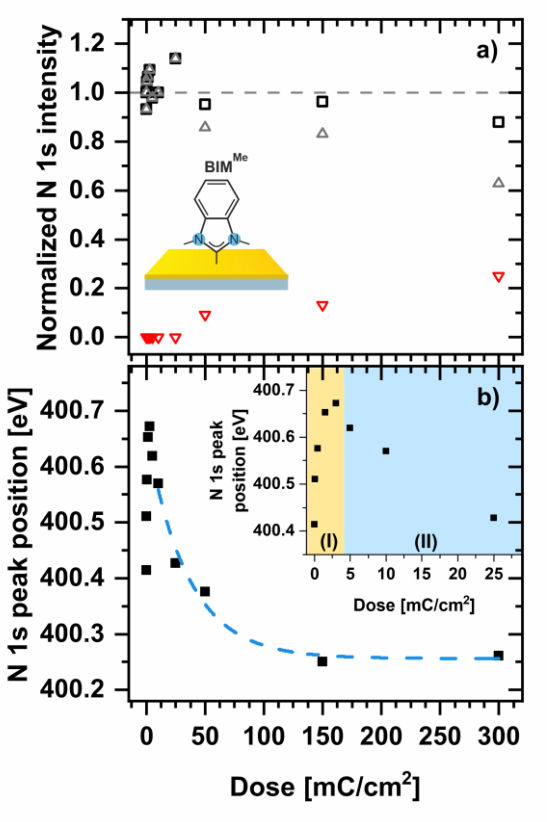

Figure 5. N 1s XPS data analysis for electron beam (50 eV) irradiated NHC SAMs. In (a) normalized intensity of total N 1s signal (black square), main component at ~400.5 eV (grey triangles) and new component at ~399-398 eV (red triangles) for BIM^{Me}/Au monlayer as a function of the total electron dose. In (b) BE of the main component of N 1s as a function of the total electron dose for BIM^{Me}/Au - the inset shows close-up for low doses indicating increase (by the cross-linking process – yellow range) and decrease (by the C–Au bond termination – blue range) of the BE value. The blue dashed line in (b) shows fitting of the saturation function (an analogue of eq. 1) to the data in the range 10-300 mC/cm^2 where the C–Au bond termination process takes place.

imidazolium unit takes place upon formation of this bond, such scenario seems much less probable as the main component in this case would be expected at lower BE (~397 eV) which is characteristic for gold nitride formation.[91] The main N 1s component exhibits also the change in the BE position during irradiation which has a similar character as for discussed above C 1s signal *i.e.* for low irradiation doses up to ~5 mC/cm^2 an increase (~0.1-0.2 eV) is observed

which for higher doses is followed by decrease showing saturation behavior (**Figure 4b**). The initial increase of the N 1s BE position is most probably caused by the cross-linking mechanism, and has been previously reported for electron irradiation (50 eV) of pyridine and pyrimidine substituted aromatic thiols.[92] The decrease in the N 1s BE (by ~0.2-0.4 eV) for higher electron doses is also correlated with the C 1s signal behavior, as it is expected assuming that destruction of the dipole layer *via* the C–Au bond termination causes the change in the electrostatic energy affecting both C and N atoms of the monolayer. Thus, the similar character of N 1s and C 1s data as a function of irradiation dose additionally supports proposed model of electron-beam-induced NHC SAMs structure modification. Moreover, fitting the N 1s data presented in **Figure 5b** and **Figure S4** at the dose range where the cross-linking process is saturated (above ~10 mC/cm^2) provides another, and independent, estimation for the respective cross-section for the C–Au bond termination (σ_{Au-C}) which for all analyzed here NHC monolayers is in the same range as calculated above from the respective C 1s data *i.e.* ~10^{-18} cm^2 (see **Table 1**).

The overall process of electron-beam-induced NHC SAMs modification is presented schematically in the upper panel of **Figure 6** including two stages of this process *i.e.* (i) the cross-linking and subsequent (ii) C–Au bond termination and N–Au bond formation. To test possible application of NHC SAMs for carbon nanomembrane (CNMs) formation the monolayers irradiated with the total dose of 150 mC/cm^2 were delaminated from the Au substrates using PMMA-based protocol[44] and transferred onto holey TEM grids, as schematically indicated in the upper panel of **Figure 6**. The quality of resulting freestanding CNMs obtained from all types of analyzed here NHC SAMs was monitored by scanning electron microscopy (SEM). Our SEM data presented in **Figure 6** show the formation of continuous CNMs in the case of BIM^{Me}/Au and NIM^{Me}/Au SAMs. In contrast, for the other two analyzed here systems *i.e.* IM^{Me}/Au and BIM^{iPr}/Au SAMs the continues CNMs are not

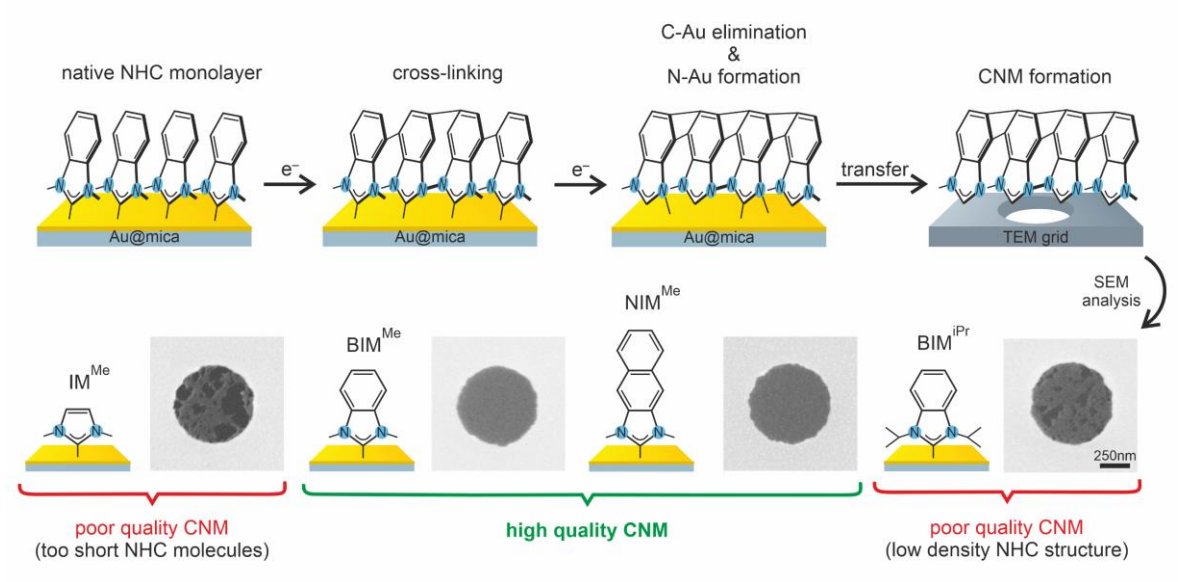

Figure 6. The upper panel shows schematic process of electron beam induced NHC SAMs modification and subsequent fabrication of the carbon nanomembranes (CNMs) that includes the following steps: (i) irradiation induced cross-linking, (ii) C–Au bonds elimination and N–Au bond formation, and (iii) delamination of the monolayer and transfer on the TEM grid. The lower panel shows representative SEM images of freestanding CNMs transferred onto holey TEM grid and obtained by irradiation of respective NHC SAM using 50 eV electron beam and total irradiation dose of 150 mC/cm^2. Continuous CNM are formed from BIM^{Me}/Au and NIM^{Me}/Au SAMs. Mesh-like CNMs with high density of large nanopores (dark patches in SEM images) are obtained for either short IM^{Me}/Au or low density BIM^{iPr}/Au monolayers.

formed revealing pores with dimensions of ~50-250 nm. These pores are a result of the low values of the cross-sections discussed earlier and presented in Table 1. For the IM^{Me}/Au the formation of nanopores is caused also by too short molecules forming this type of monolayer and thus in a lower mechanical stability of the resulting CNM which is then can be easily ruptured during delamination process and subsequent transfer onto the TEM grid. For BIM^{iPr}/Au the length of the molecule's forming this monolayer is expected to be sufficient, as confirmed by formation of continues CNMs obtained for analogues BIM^{Me}/Au monolayer.

However, a continues CNM is not formed resulting from the increased size of intermolecular distance between the molecules due to presence of the side groups which are limiting efficiency of the cross-linking process as discussed earlier.

4. Summary and Conclusions

Detailed XPS analysis of electron irradiated NHC SAMs (IM^{Me}/Au, BIM^{Me}/Au, NIM^{Me}/Au and BIM^{iPr}/Au), revealed the basic mechanism of modification of these systems by low-energy (50 eV) beam and its dependence on the structure of precursors. Our analysis shows that similar to other aromatic SAMs the NHC monolayers undergo cross-linking process with a relatively small reduction of the film thickness (~20-10%), even for the systems which are exclusively based on using imidazolium unit without any aromatic moiety. The measured cross-section for the film thickness reduction (~10^{-16} cm^2), which is higher for systems with higher efficiency of the cross-linking process, grows with the number n (n = 0-2) of phenyl rings in the molecules forming NHC monolayers (IM^{Me}/Au < BIM^{Me}/Au < NIM^{Me}/Au). At the same time this parameter, and thus the cross-linking process, is strongly reduced for analogues NHC monolayers (BIM^{iPr}/Au < BIM^{Me}/Au) where short methyl (Me) side groups were substituted by a bulkier isopropyl (iPr). In both cases such behavior can be rationalized assuming, a higher cross-linking probability for longer aromatic molecules, and lower cross-linking probability for larger separation between molecules controlled by the size of the side groups, respectively. Another process, which takes over at higher doses of electron irradiation, is elimination of the C–Au bonds between molecules forming NHC SAM and the Au substrate. Importantly, the measured cross-section for this process (~10^{-18} cm^2) is by one or two orders of magnitude lower compared to aromatic SAMs based on thiol or carboxylic bonding group indicating much higher stability towards electron irradiation of the C–Au bond compared to S–Au or O–Au, respectively. The estimated fraction of the C–Au bonding groups, which are eliminated in the

NHC SAMs, also depends on their structure at the molecule-metal interface and is higher for IM^{Me}/Au and BIM^{iPr}/Au compared to BIM^{Me}/Au and NIM^{Me}/Au following also former analysis of their thermal stability. Together with elimination of the original C–Au bond our data indicate that during irradiation a new bonding with the substrate is activated *via* formation of the N–Au bond which is a result of electron-induced modification of the imidazolium moiety. Finally, the analysis of delamination and transferring of electron-irradiated NHC monolayers on holey TEM grid reveals formation of freestanding CNMs. Continuous CNMs are formed for BIM^{Me}/Au and NIM^{Me}/Au systems. Application of shorter molecules (IM^{Me}/Au) or having more bulky nitrogen side groups (BIM^{iPr}/Au) results in high density of nanopores and the fabrication of mesh-like CNMs. These observations are fully correlated with the structurally controlled efficiency of the cross-linking process which determines mechanical stability of the CNMs during their delamination and transferring.

To conclude, our results provide design rules to optimize NHC SAMs structure for their effective modification by electron irradiation. Such optimization becomes particularly interesting considering that NHC monolayers provide much higher stability of their bonding with the metal substrate towards electron irradiation compared to standard thiols or recently investigated carboxylic acids. Thus, NHC monolayers offer an interesting alternative for chemical lithography where structural modification of SAMs by electron or photon beams (considering that primary damage in SAMs induced by X-ray, UV or EUV irradiation is due to photo and secondary electrons)[21,93] should be limited mainly to the terminal group keeping bonding with the substrate mostly intact.[27,34,36,94,95] Another important advantage of NHC SAMs in the context of electron-induced modification, which is also highly sensitive to their design, is their application for sulfur-free CNM fabrication as a much more stable alternative for recently proposed carboxylic SAMs.[44–47]

Supporting Information. Figures S1–S4 indicated in the manuscript.

Acknowledgments

PC thank Priority Research Area SciMat under the program Excellence Initiative – Research University at the Jagiellonian University in Kraków. This work was supported financially by the National Science Centre Poland (grant DEC-2018/31/B/ST5/00057) and by Deutsche Forschungsgemeinschaft (grants CRC "CataLight" B7 and Z2).

References

(1) Love, J. C.; Estroff, L. A.; Kriebel, J. K.; Nuzzo, R. G.; Whitesides, G. M. Self-Assembled Monolayers of Thiolates on Metals as a Form of Nanotechnology. *Chem. Rev.* **2005**, *105* (4), 1103–1170.

(2) Gooding, J. J.; Ciampi, S. The Molecular Level Modification of Surfaces: From Self-Assembled Monolayers to Complex Molecular Assemblies. *Chem. Soc. Rev.* **2011**, *40* (5), 2704–2718.

(3) Vericat, C.; Vela, M. E.; Benitez, G.; Carro, P.; Salvarezza, R. C. Self-Assembled Monolayers of Thiols and Dithiols on Gold: New Challenges for a Well-Known System. *Chem. Soc. Rev.* **2010**, *39* (5), 1805–1834.

(4) Buriak, J. M.; Chan, W. C. W.; Chen, X.; Hersam, M. C.; Liz-Marzán, L. M.; Weiss, P. S. The 2022 Kavli Prize in Nanoscience: Self-Assembled Monolayers. *ACS Nano* **2022**, 16 (7), 9965–9967.

(5) Smith, R. K.; Lewis, P. A.; Weiss, P. S. Patterning Self-Assembled Monolayers. *Prog. Surf. Sci.* **2004**, 75, (1-2), 1–68.

(6) Singh, M.; Kaur, N.; Comini, E. The Role of Self-Assembled Monolayers in Electronic Devices. *J. Mater. Chem. C*. **2020**, 8, 3938–3955.

(7) Schmaltz, T.; Sforazzini, G.; Reichert, T.; Frauenrath, H. Self-Assembled Monolayers as Patterning Tool for Organic Electronic Devices. *Advanced Materials* **2017**, 29 (18), 1605286.

(8) Vilan, A.; Aswal, D.; Cahen, D. Large-Area, Ensemble Molecular Electronics: Motivation and Challenges. *Chem. Rev.* **2017**, *117* (5), 4248–4286.

(9) Metzger, R. M. Unimolecular Electronics. *Chem. Rev.* **2015**, 115 (11), 5056–5115.

(10) Metzger, R. M. Quo Vadis, Unimolecular Electronics? *Nanoscale* **2018**, 10, 10316–10332.

(11) Casalini, S.; Bortolotti, C. A.; Leonardi, F.; Biscarini, F. Self-Assembled Monolayers in Organic Electronics. *Chem. Soc. Rev.* **2017**, 46, 40–71.

(12) Gupta, R.; Fereiro, J. A.; Bayat, A.; Protam, A.; Zharnikov, M.; Mondal, P. C. Nanoscale Molecular Rectifiers. *Nat. Rev. Chem.* **2023**, *7* (2), 106–122.

(13) Cui, H.; Wang, W.; Shi, L.; Song, W.; Wang, S. Superwettable Surface Engineering in Controlling Cell Adhesion for Emerging Bioapplications. *Small Methods* **2020**, 4, 202000573.

(14) Dai, Y.; Liu, C. C. Recent Advances on Electrochemical Biosensing Strategies toward Universal Point-of-Care Systems. *Angew. Chem. Int. Ed.* **2019**, *58* (36), 12355–12368.

(15) Irimia-Vladu, M. "Green" Electronics: Biodegradable and Biocompatible Materials and Devices for Sustainable Future. *Chem. Soc. Rev.* **2014**, 43, 588–610.

(16) Bauer, S.; Schmuki, P.; von der Mark, K.; Park, J. Engineering Biocompatible Implant Surfaces: Part I: Materials and Surfaces. *Prog. Mater. Sci.* **2013**, 58 (3), 261–326.

(17) Mu, H. U.; Zharnikov, M.; Vo, B.; Schertel, A.; Harder, P.; Grunze, M. Low-Energy Electron-Induced Damage in Hexadecanethiolate Monolayers. *J. Phys. Chem. B* **1998**, 102 (41), 7949-7959.

(18) Zharnikov, M.; Frey, S.; Heister, K.; Grunze, M. Modification of Alkanethiolate Monolayers by Low Energy Electron Irradiation: Dependence on the Substrate Material and on the Length and Isotopic Composition of the Alkyl Chains. *Langmuir* **2000**, *16* (6), 2697–2705.

(19) Schmid, M.; Wan, X.; Asyuda, A.; Zharnikov, M. Modification of Self-Assembled Monolayers by Electron Irradiation: The Effect of Primary Energy (10-500 EV). *J. Phys. Chem. C* **2019**, *123* (46), 28301–28309.

(20) Geyer, W.; Stadler, V.; Eck, W.; Zharnikov, M.; Gö Lzhä, A.; Grunze, M. Electron-Induced Crosslinking of Aromatic Self-Assembled Monolayers: Negative Resists for Nanolithography. *Appl. Phys. Lett.* 1999, 53(17), 1660-1662.

(21) Zharnikov, M.; Grunze, M. Modification of Thiol-Derived Self-Assembling Monolayers by Electron and x-Ray Irradiation: Scientific and Lithographic Aspects. *J. Vac. Sci. Techol. B* **2002**, *20* (5), 1793.

(22) Cyganik, P.; Vandeweert, E.; Postawa, Z.; Bastiaansen, Z.; Vervaecke, F.; Lievens, P.; Silverans, R. E.; Winograd, N. Modification and Stability of Aromatic Self-Assembled Monolayers upon Irradiation with Energetic Particles. *J. Phys. Chem. B* **2005**, *109* (11), 5085–5094.

(23) Turchanin, A.; Käfer, D.; El-Desawy, M.; Wöll, C.; Witte, G.; Gölzhäuser, A. Molecular Mechanisms of Electron-Induced Cross-Linking in Aromatic SAMs. *Langmuir* **2009**, *25* (13), 7342–7352.

(24) Neumann, C.; Wilhelm, R. A.; Küllmer, M.; Turchanin, A. Low-Energy Electron Irradiation Induced Synthesis of Molecular Nanosheets: Influence of the Electron Beam Energy. *Faraday Discuss.* **2021**, *227*, 61–79.

(25) Eck, W.; Stadler, V.; Geyer, W.; Zharnikov, M.; Gölzhäuser, A.; Grunze, M. Generation of Surface Amino Groups on Aromatic Self-Assembled Monolayers by Low Energy Electron Beams – A First Step Towards Chemical Lithography. *Adv. Mater.* **2000**, *12 (11)*, 805–808.

(26) Terfort, A.; Zharnikov, M. Electron-Irradiation Promoted Exchange Reaction as a Tool for Surface Engineering and Chemical Lithography. *Adv. Mater. Interances* **2021**, 8, 2100148.

(27) Schilp, S.; Ballav, N.; Zharnikov, M. Fabrication of a Full-Coverage Polymer Nanobrush on an Electron-Beam- Activated Template. *Angew. Chem. Int. Ed.* **2008**, *47* (36), 6786–6789.

(28) Ballav, N.; Schilp, S.; Zharnikov, M. Electron-Beam Chemical Lithography with Aliphatic Self-Assembled Monolayers. *Angew. Chem. Int. Ed.* **2008**, *47* (8), 1421–1424.

(29) Turchanin, A.; El-Desawy, M.; Gölzhäuser, A. High Thermal Stability of Cross-Linked Aromatic Self-Assembled Monolayers: Nanopatterning via Selective Thermal Desorption. *Appl. Phys. Lett.* **2007**, *90* (5).

(30) Turchanin, A.; Tinazli, A.; El-Desawy, M.; Großmann, H.; Schnietz, M.; Solak, H. H.; Tampé, R.; Gölzhäuser, A. Molecular Self-Assembly, Chemical Lithography, and Biochemical Tweezers: A Path for the Fabrication of Functional Nanometer-Scale Protein Arrays. *Adv. Mater.* **2008**, *20* (3), 471–477.

(31) Ballav, N.; Thomas, H.; Winkler, T.; Terfort, A.; Zharnikov, M. Making Protein Patterns by Writing in a Protein-Repelling Matrix. *Angew. Chem. Int. Ed.* **2009**, *48* (32), 5833–5836.

(32) Küller, A.; Eck, W.; Stadler, V.; Geyer, W.; Gölzhäuser, A. Nanostructuring of Silicon by Electron-Beam Lithography of Self-Assembled Hydroxybiphenyl Monolayers. *Appl. Phys. Lett.* **2003**, *82* (21), 3776–3778.

(33) Zhao, Z.; Fukushima, T.; Zharnikov, M. Electron-Induced Modification of Triptycene Self-Assembled Monolayers in Context of Lithography and Nanofabrication. *J. Phys. Chem. C* **2023**, *127* (31), 15582–15590.

(34) Gölzhäuser, A.; Eck, W.; Geyer, W.; Stadler, V.; Weimann, T.; Hinze, P.; Grunze, M. Chemical Nanolithography with Electron Beams. *Adv. Mater.* **2001**, *13* (11), 803–806.

(35) Weber, N. E.; Wundrack, S.; Stosch, R.; Turchanin, A. Direct Growth of Patterned Graphene. *Small* **2016**, *12* (11), 1440–1445.

(36) Sauter, E.; Yildirim, C.; Terfort, A.; Zharnikov, M. Adjustment of the Work Function of Pyridine and Pyrimidine Substituted Aromatic Self-Assembled Monolayers by Electron Irradiation. *J. Phys. Chem. C* **2017**, *121* (23), 12834–12841.

(37) Matei, D. G.; Weber, N. E.; Kurasch, S.; Wundrack, S.; Woszczyna, M.; Grothe, M.; Weimann, T.; Ahlers, F.; Stosch, R.; Kaiser, U.; Turchanin, A. Functional Single-Layer Graphene Sheets from Aromatic Monolayers. *Adv. Mater.* **2013**, *25* (30), 4146–4151.

(38) Neumann, C.; Kaiser, D.; Mohn, M. J.; Fuser, M.; Weber, N. E.; Reimer, O.; Gölzhäuser, A.; Weimann, T.; Terfort, A.; Kaiser, U.; Turchanin, A. Bottom-Up Synthesis of

Graphene Monolayers with Tunable Crystallinity and Porosity. *ACS Nano* **2019**, *13* (6), 7310–7322.

(39) Turchanin, A.; Gölzhäuser, A. Carbon Nanomembranes from Self-Assembled Monolayers: Functional Surfaces without Bulk. *Prog. Surf. Sci.* 2012, 87 (5-8), 108–162.

(40) Turchanin, A.; Beyer, A.; Nottbohm, C. T.; Zhang, X.; Stosch, R.; Sologubenko, A.; Mayer, J.; Hinze, P.; Weimann, T.; Gölzhäuser, A. One Nanometer Thin Carbon Nanosheets with Tunable Conductivity and Stiffness. *Adv. Mater.* **2009**, *21* (12), 1233–1237.

(41) Turchanin, A.; Gölzhäuser, A. Carbon Nanomembranes. *Adv. Mater.***2016**, 28 (29), 6075–6103.

(42) Angelova, P.; Vieker, H.; Weber, N. E.; Matei, D.; Reimer, O.; Meier, I.; Kurasch, S.; Biskupek, J.; Lorbach, D.; Wunderlich, K.; Chen, L.; Terfort, A.; Klapper, M.; Müllen, K.; Kaiser, U.; Gölzhäuser, A.; Turchanin, A. A Universal Scheme to Convert Aromatic Molecular Monolayers into Functional Carbon Nanomembranes. *ACS Nano* **2013**, *7* (8), 6489–6497.

(43) Turchanin A. Synthesis of Molecular 2D Materials via Low-Energy Electron Induced Chemical Reactions. *Chimia* **2019**, *73*, 473–479.

(44) Neumann, C.; Szwed, M.; Frey, M.; Tang, Z.; Kozieł, K.; Cyganik, P.; Turchanin, A. Preparation of Carbon Nanomembranes without Chemically Active Groups. *ACS Appl. Mater. Interfaces* **2019**, *11* (34), 31176–31181.

(45) Kruk, M.; Neumann, C.; Frey, M.; Kozieł, K.; Turchanin, A.; Cyganik, P. Odd-Even Effect in Electron Beam Irradiation of Hybrid Aromatic - Aliphatic Self-Assembled Monolayers of Fatty Acid. *J. Phys. Chem. C* **2021**, *125* (17), 9310–9318.

(46) Dementyev, P.; Naberezhnyi, D.; Westphal, M.; Buck, M.; Gölzhäuser, A. Carbon Nanomembranes from Aromatic Carboxylate Precursors. *ChemPhysChem* **2020**, *21* (10), 1006–1011.

(47) Asyuda, A.; De La Morena, R. O.; Sauter, E.; Turner, K.; McDonald, K.; Buck, M.; Zharnikov, M. Electron-Induced Modification of Self-Assembled Monolayers of Aromatic Carboxylic Acids. *J. Phys. Chem. C* **2020**, *124* (45), 25107–25120.

(48) Yang, Y.; Dementyev, P.; Biere, N.; Emmrich, D.; Stohmann, P.; Korzetz, R.; Zhang, X.; Beyer, A.; Koch, S.; Anselmetti, D.; Gölzhäuser, A. Rapid Water Permeation Through Carbon Nanomembranes with Sub-Nanometer Channels. *ACS Nano* **2018**, *12* (5), 4695–4701.

(49) Ai, M.; Shishatskiy, S.; Wind, J.; Zhang, X.; Nottbohm, C. T.; Mellech, N.; Winter, A.; Vieker, H.; Qiu, J.; Dietz, K. J.; Gölzhäuser, A.; Beyer, A. Carbon Nanomembranes (CNMs) Supported by Polymer: Mechanics and Gas Permeation. *Adv. Mater.* **2014**, *26* (21), 3421–3426.

(50) Hamann, T.; Kankate, L.; Böhler, E.; Bredehöft, J. H.; Zhang, F. M.; Gölzhäuser, A.; Swiderek, P. Functionalization of a Self-Assembled Monolayer Driven by Low-Energy Electron Exposure. *Langmuir* **2012**, *28* (1), 367–376.

(51) Zheng, Z.; Nottbohm, C. T.; Turchanin, A.; Muzik, H.; Beyer, A.; Heilemann, M.; Sauer, M.; Gölzhäuser, A. Janus Nanomembranes: A Generic Platform for Chemistry in Two Dimensions. *Angew. Chem. Int. Ed.* **2010**, *49* (45), 8493–8497.

(52) Crudden, C. M.; Horton, J. H.; Ebralidze, I. I.; Zenkina, O. V.; McLean, A. B.; Drevniok, B.; She, Z.; Kraatz, H. B.; Mosey, N. J.; Seki, T.; Keske, E. C.; Leake, J. D.; Rousina-Webb, A.; Wu, G. Ultra Stable Self-Assembled Monolayers of N-Heterocyclic Carbenes on Gold. *Nat. Chem.* **2014**, *6* (5), 409–414.

(53) Crudden, C. M.; Horton, J. H.; Narouz, M. R.; Li, Z.; Smith, C. A.; Munro, K.; Baddeley, C. J.; Larrea, C. R.; Drevniok, B.; Thanabalasingam, B.; McLean, A. B.; Zenkina, O. V.; Ebralidze, I. I.; She, Z.; Kraatz, H. B.; Mosey, N. J.; Saunders, L. N.; Yagi, A. Simple Direct Formation of Self-Assembled N-Heterocyclic Carbene Monolayers on Gold and Their Application in Biosensing. *Nat. Commun.* **2016**, *7*, 12654.

(54) Dominique, N. L.; Chandran, A.; Jensen, I. M.; Jenkins, D. M.; Camden, J. P. Unmasking the Electrochemical Stability of N-Heterocyclic Carbene Monolayers on Gold. *Chem. Eur. J.* **2024**, 30, e202303681.

(55) Larrea, C. R.; Baddeley, C. J.; Narouz, M. R.; Mosey, N. J.; Horton, J. H.; Crudden, C. M. N-Heterocyclic Carbene Self-Assembled Monolayers on Copper and Gold: Dramatic Effect of Wingtip Groups on Binding, Orientation and Assembly. *ChemPhysChem* **2017**, *18* (24), 3536–3539.

(56) Krzykawska, A.; Wróbel, M.; Kozieł, K.; Cyganik, P. N-Heterocyclic Carbenes for the Self-Assembly of Thin and Highly Insulating Monolayers with High Quality and Stability. *ACS Nano* **2020**, *14* (5), 6043–6057.

(57) Wróbel, M.; Cegiełka, D. M.; Asyuda, A.; Kozieł, K.; Zharnikov, M.; Cyganik, P. N-Heterocyclic Carbenes – The Design Concept for Densely Packed and Thermally Ultra-Stable Aromatic Self-Assembled Monolayers. *Nano Today* **2023**, *53*, 102024.

(58) Engel, S.; Fritz, E. C.; Ravoo, B. J. New Trends in the Functionalization of Metallic Gold: From Organosulfur Ligands to N-Heterocyclic Carbenes. *Chem. Soc. Rev.* **2017**, 46, 2057–2075.

(59) Smith, C. A.; Narouz, M. R.; Lummis, P. A.; Singh, I.; Nazemi, A.; Li, C. H.; Crudden, C. M. N-Heterocyclic Carbenes in Materials Chemistry. *Chem. Rev.* **2019**, 119 (8), 4986–5056.

(60) Koy, M.; Bellotti, P.; Das, M.; Glorius, F. N-Heterocyclic Carbenes as Tunable Ligands for Catalytic Metal Surfaces. *Nat. Catal.* **2021**, 4, 352–363.

(61) Kaur, G.; Thimes, R. L.; Camden, J. P.; Jenkins, D. M. Fundamentals and Applications of N-Heterocyclic Carbene Functionalized Gold Surfaces and Nanoparticles. *Chem. Comm.* **2022**, *58* (95), 13188–13197.

(62) Sherman, L. M.; Strausser, S. L.; Borsari, R. K.; Jenkins, D. M.; Camden, J. P. Imidazolinium N-Heterocyclic Carbene Ligands for Enhanced Stability on Gold Surfaces. *Langmuir* **2021**, *37* (19), 5864–5871.

(63) Bakker, A.; Freitag, M.; Kolodzeiski, E.; Bellotti, P.; Timmer, A.; Ren, J.; Schulze Lammers, B.; Moock, D.; Roesky, H. W.; Mönig, H.; Amirjalayer, S.; Fuchs, H.; Glorius, F.

An Electron-Rich Cyclic (Alkyl)(Amino)Carbene on Au(111), Ag(111), and Cu(111) Surfaces. *Angew. Chem. Int. Ed.* **2020**, *59* (32), 13643–13646.

(64) Amit, E.; Berg, I.; Gross, E. Self-Assembled Monolayers of Nitron: Self-Activated and Chemically Addressable N-Heterocyclic Carbene Monolayers with Triazolone Structural Motif. *Chem. Eur. J.* **2020**, *26* (57), 13046–13052.

(65) Gutheil, C.; Roß, G.; Amirjalayer, S.; Mo, B.; Schäfer, A. H.; Doltsinis, N. L.; Braunschweig, B.; Glorius, F. Tailored Monolayers of N-Heterocyclic Carbenes by Kinetic Control. *ACS Nano* **2024**, *18*, 3043–3052.

(66) Kim, K. H.; Seo, S. E.; Park, S. J.; Kim, J.; Park, C. S.; Le, T. H.; Lee, C. S.; Kim, Y. K.; Kim, H. Y.; Jun, S.; Kwak, J.; Lee, Y. K.; Yoon, H.; Song, H. S.; Kwon, O. S. N-Heterocyclic Carbene–Graphene Nanotransistor Based on Covalent Bond for Ultrastable Biosensors. *Adv Funct Mater* **2024**.

(67) Park, S.; Kang, S.; Yoon, H. J. Thermopower of Molecular Junction in Harsh Thermal Environments. *Nano Lett* **2022**, *22* (10), 3953–3960.

(68) Jain, M.; Gerstmann, U.; Schmidt, W. G.; Aldahhak, H. Adatom Mediated Adsorption of N-Heterocyclic Carbenes on Cu(111) and Au(111). *J. Comput. Chem.* **2022**, *43* (6), 413–420.

(69) Inayeh, A.; Groome, R. R. K.; Singh, I.; Veinot, A. J.; de Lima, F. C.; Miwa, R. H.; Crudden, C. M.; McLean, A. B. Self-Assembly of N-Heterocyclic Carbenes on Au(111). *Nat. Commun.* **2021**, *12* (1).

(70) Lovat, G.; Doud, E. A.; Lu, D.; Kladnik, G.; Inkpen, M. S.; Steigerwald, M. L.; Cvetko, D.; Hybertsen, M. S.; Morgante, A.; Roy, X.; Venkataraman, L. Determination of the Structure and Geometry of N-Heterocyclic Carbenes on Au(111) Using High-Resolution Spectroscopy. *Chem. Sci.* **2019**, *10* (3), 930–935.

(71) Dery, S.; Kim, S.; Tomaschun, G.; Haddad, D.; Cossaro, A.; Verdini, A.; Floreano, L.; Klüner, T.; Toste, F. D.; Gross, E. Flexible NO2-Functionalized N-Heterocyclic Carbene Monolayers on Au (111) Surface. *Chem. Eur. J.* **2019**, 25 (66), 15067-15072.

(72) Tang, Q.; Jiang, D. E. Comprehensive View of the Ligand-Gold Interface from First Principles. *Chem. Mater.* **2017**, *29* (16), 6908–6915.

(73) Angove, E.; Grillo, F.; Früchtl, H. A.; Veinot, A. J.; Singh, I.; Horton, J. H.; Crudden, C. M.; Baddeley, C. J. Highly Ordered N-Heterocyclic Carbene Monolayers on Cu(111). *J. Phys. Chem. Lett.* **2022**, *13* (8), 2051–2056.

(74) Ossowski, J.; Wächter, T.; Silies, L.; Kind, M.; Noworolska, A.; Blobner, F.; Gnatek, D.; Rysz, J.; Bolte, M.; Feulner, P.; Terfort, A.; Cyganik, P.; Zharnikov, M. Thiolate versus Selenolate: Structure, Stability, and Charge Transfer Properties. *ACS Nano* **2015**, *9* (4), 4508–4526.

(75) Cyganik, P.; Buck, M.; Strunskus, T.; Shaporenko, A.; Wilton-Ely, J. D. E. T.; Zharnikov, M.; Wöll, C. Competition as a Design Concept: Polymorphism in Self-Assembled Monolayers of Biphenyl-Based Thiols. *J. Am. Chem. Soc.* **2006**, *128* (42), 13868–13878.

(76) Wróbel, M.; Żaba, T.; Sauter, E.; Krawiec, M.; Sobczuk, J.; Terfort, A.; Zharnikov, M.; Cyganik, P. Thermally Stable and Highly Conductive SAMs on Ag Substrate—The Impact of the Anchoring Group. *Adv. Electron. Mater.* **2021**, *7* (2).

(77) Shaporenko, A.; Cyganik, P.; Buck, M.; Terfort, A.; Zharnikov, M. Self-Assembled Monolayers of Aromatic Selenolates on Noble Metal Substrates. *J. Phys. Chem. B* **2005**, *109* (28), 13630–13638.

(78) Taucher, T. C.; Hehn, I.; Hofmann, O. T.; Zharnikov, M.; Zojer, E. Understanding Chemical versus Electrostatic Shifts in X-Ray Photoelectron Spectra of Organic Self-Assembled Monolayers. *J. Phys. Chem. C* **2016**, *120* (6), 3428–3437.

(79) Chang, K.; Chen, J. G.; Lu, Q.; Cheng, M. J. Quantum Mechanical Study of N-Heterocyclic Carbene Adsorption on Au Surfaces. *J. Phys. Chem. A* **2017**, *121* (13), 2674–2682.

(80) Rodríguez-Castillo, M.; Lugo-Preciado, G.; Laurencin, D.; Tielens, F.; van der Lee, A.; Clément, S.; Guari, Y.; López-de-Luzuriaga, J. M.; Monge, M.; Remacle, F.; Richeter, S. Experimental and Theoretical Study of the Reactivity of Gold Nanoparticles Towards Benzimidazole-2-Ylidene Ligands. *Chem. Eur. J.* **2016**, *22* (30), 10446–10458.

(81) Yildirim, C.; Füser, M.; Terfort, A.; Zharnikov, M. Modification of Aromatic Self-Assembled Monolayers by Electron Irradiation: Basic Processes and Related Applications. *J. Phys. Chem. C* **2017**, *121* (1), 567–576.

(82) Weidner, T.; Ballav, N.; Grunze, M.; Terfort, A.; Zharnikov, M. Modification of Biphenylselenolate Monolayers by Low-Energy Electrons. *Phys. Status Solidi B* **2009**, *246* (7), 1519–1528.

(83) De Boer, B.; Hadipour, A.; Mandoc, M. M.; Van Woudenbergh, T.; Blom, P. W. M. Tuning of Metal Work Functions with Self-Assembled Monolayers. *Adv. Mater.* **2005**, *17* (5), 621–625.

(84) Heimel, G.; Romaner, L.; Zojer, E.; Bredas, J. L. Toward Control of the Metal-Organic Interfacial Electronic Structure in Molecular Electronics: A First-Principles Study on Self-Assembled Monolayers of π-Conjugated Molecules on Noble Metals. *Nano Lett.* **2007**, *7* (4), 932–940.

(85) Heimel, G.; Romaner, L.; Zojer, E.; Bredas, J. L. The Interface Energetics of Self-Assembled Monolayers on Metals. *Acc. Chem. Res.* **2008**, 41 (6), 721–729.

(86) Olsen, C.; Rowntree, P. A. Bond-Selective Dissociation of Alkanethiol Based Self-Assembled Monolayers Adsorbed on Gold Substrates, Using Low-Energy Electron Beams; *J. Chem. Phys.* **1998**, 108, 3750–3764.

(87) Avouris, P.; Persson, B. N. J. Excited States at Metal Surfaces and Their Nonradiative Relaxation; *J. Phys. Chem.* **1984**, 88 (5), 837–848.

(88) Gallardo, I.; Pinson, J.; Vilà, N. Spontaneous Attachment of Amines to Carbon and Metallic Surfaces. *J. Phys. Chem. B* **2006**, *110* (39), 19521–19529.

(89) Tian, L.; Martine, E.; Yu, X.; Hu, W. Amine-Anchored Aromatic Self-Assembled Monolayer Junction: Structure and Electric Transport Properties. *Langmuir* **2021**, *37* (41), 12223–12233.

(90) Herrer, L.; Ismael, A.; Martín, S.; Milan, D. C.; Serrano, J. L.; Nichols, R. J.; Lambert, C.; Cea, P. Single Molecule vs. Large Area Design of Molecular Electronic Devices Incorporating an Efficient 2-Aminepyridine Double Anchoring Group. *Nanoscale* **2019**, *11* (34), 15871–15880.

(91) Šiller, L.; Alves, L.; Brieva, A. C.; Butenko, Y. V.; Hunt, M. R. C. Gold Nitride: Preparation and Properties. *Top. Catal.* **2009**, 52, 1604–1610.

(92) Sauter, E.; Yildirim, C.; Terfort, A.; Zharnikov, M. Adjustment of the Work Function of Pyridine and Pyrimidine Substituted Aromatic Self-Assembled Monolayers by Electron Irradiation. *J. Phys. Chem. C* **2017**, *121* (23), 12834–12841.

(93) Turchanin, A.; Schnietz, M.; El-Desawy, M.; Solak, H. H.; David, C.; Gölzhäuser, A. Fabrication of Molecular Nanotemplates in Self-Assembled Monolayers by Extreme-Ultraviolet-Induced Chemical Lithography. *Small* **2007**, *3* (12), 2114–2119.

(94) Jeyachandran, Y. L.; Terfort, A.; Zharnikov, M. Controlled Modification of Protein-Repelling Self-Assembled Monolayers by Ultraviolet Light: The Effect of the Wavelength. *J. Phys. Chem. C* **2012**, *116* (16), 9019–9028.

(95) Jeyachandran, Y. L.; Meyerbroker, N.; Terfort, A.; Zharnikov, M. Maskless Ultraviolet Projection Lithography with a Biorepelling Monomolecular Resist. *J. Phys. Chem. C* **2015**, *119* (1), 494–501.